Available online at www.sciencedirect.com
ScienceDirect
International Journal of Heat and Fluid Flow 29 (2008) 903–915
International Journal of HEAT AND FLUID FLOW
www.elsevier.com/locate/ijhff

The influence of wall heating on the flow structure in the near-wall region

Shivani T. Gajusingh, M.H. Kamran Siddiqui *

Department of Mechanical and Industrial Engineering, Concordia University, Montreal, QC, Canada H3G 1M8

Received 14 June 2007; received in revised form 7 November 2007; accepted 9 January 2008
Available online 3 March 2008

Abstract

The impact of wall heating on the flow structure in the near-wall region inside a square channel was investigated. PIV was used to measure the two-dimensional velocity fields. The measurements were conducted for a range of flow conditions that covers laminar and turbulent regimes. The results have shown that the impact of wall heating on the flow behavior is significantly different for laminar and turbulent flow regimes. It was found that when an originally laminar flow is heated from below, the turbulence is generated in the flow mainly due to buoyancy. When the flow is in the turbulent regime, addition of heat from below reduces the magnitude of turbulent properties due to the working of turbulence against the buoyancy forces. Results also show that for originally laminar flow, an increase in the instability in stratification increases the turbulence whereas, for originally turbulent flows, the turbulence is decreased with an increase in instability.

Keywords: Wall heating; Turbulent structure; Square channel; Near-wall region

1. Introduction

Significant work has been done over the past several decades, to understand the internal flows and the flow structure over a solid wall. These studies can broadly be categorized into two groups. The first group is focused on the investigation of the flow structure in an unheated channel or above an unheated wall. Of particular interest was the impact of wall roughness on the flow structure in the inner and outer layers adjacent to the wall. The results showed that the surface roughness has an impact on the wall shear stress and near-surface turbulent properties. However, there is no consensus on the extent from the wall up to which the influence of surface roughness is significant. Some studies supported the Townsend's (1976) similarity hypothesis that at sufficiently high Reynolds number, the turbulent flow in the region outside the roughness sublayer is independent of the wall roughness (for example, Perry et al., 1987; Bakken et al., 2005). Whereas, other studies observed the impact of wall roughness in the outer layer (for example, Krogstad et al., 1992; Bergstrom et al., 2002). There were also several studies focused on the flow behavior over smooth walls. For example, Gerard (1974) studied the turbulent flow over a smooth wall and observed the existence of the mean streamwise vorticity. Na et al. (2001) studied the Reynolds stresses and turbulence production associated with vortices over a smooth wall. Del Alamo et al. (2004) proposed scaling for logarithmic and outer layers over smooth walls. They argued that the width of the streamwise structures scales with their length and that the appropriate velocity scale of the largest streamwise structure is the centerline velocity instead of the friction velocity.

The second group is focused on the investigation of the flow and thermal structure when heat is added from the wall. Nicholl (1970) studied the effects of heat on a turbulent boundary layer for stable and unstable stratifications in a wind tunnel. The wall and free stream temperature

* Corresponding author. Tel.: +1 514 848 2424x7940; fax: +1 514 848 3175.
E-mail address: siddiqui@encs.concordia.ca (M.H. Kamran Siddiqui).

0142-727X/$ - see front matter © 2008 Elsevier Inc. All rights reserved.
doi:10.1016/j.ijheatfluidflow.2008.01.003

difference ranged from 20 to 100 °C. He observed that for unstable stratification, the mean velocity and turbulent intensities near the upstream edge of the heated plate are larger in magnitude than that observed further downstream. He argued that when the boundary layer first encounters the heated surface, the interaction of convective layer and boundary layer turbulence induce intense local convective activity, which reduces with the downstream distance. At a distance of 74 cm from the upstream heated edge, he compared the mean and turbulent intensity profiles for heated and unheated conditions and observed no significant difference in the magnitudes. Arya (1975) investigated the effects of buoyancy on the mean and turbulence structure in a developed turbulent flow over a horizontal flat plate. Experiments were conducted for stable, neutral and unstable conditions. He observed that the thickness of the viscous sublayer increased with stability, whereas, the coefficients of skin friction and heat transfer decreased with stability. The turbulence characteristics, however, were presented only for stably stratified conditions and it was concluded that the turbulence was suppressed with increasing stability. Perry and Hoffmann (1976) investigated the flow over a constant temperature wall to determine the scaling laws for the mean and fluctuating temperature and velocities using X-wire probes. They showed that the temperature and velocity profiles correlate well with inner and outer layers scaling. They also observed that the fluctuating properties are more sensitive to spurious pressure gradients than the mean flow. Rued et al. (1987) conducted experimental and numerical investigation of the flow in a square channel with one heated wall. The velocity field was measured using laser Doppler anemometry. Their study was focused on the effects of wall intersections (i.e. the corner effects) on the flow and heat transfer. They observed an increase in the Nusselt number in the corner region of the channel where the heated and unheated walls intersect. They attributed this enhanced heat transfer to non-symmetry and anisotropy at the corner and the proximity of the unheated wall.

Fukui and Nakajima (1985) investigated the impact of unstable thermal stratification on the flow and thermal structure in the wall region. They measured velocity and temperature fluctuations in the wall region of fully developed turbulent flow between horizontal parallel plates for a range of Reynolds and Richardson numbers. They found that in the inner region, the normalized horizontal velocity fluctuations increase with an increase in the Richardson number. The opposite trend was observed for the vertical velocity fluctuations in the inner region. That is, the normalized velocity magnitude decreased with an increase in the Richardson number. In the outer region, the horizontal velocity fluctuations collapsed for all cases, whereas, the trend of the vertical velocity fluctuations was reversed. That is, the vertical velocity magnitude increased with the Richardson number. They concluded that during unstable stratification, the dependency of the turbulent intensities differ in the inner and outer regions. They also observed that unstable stratification has no effect on the temperature fluctuation in the inner region but the magnitude of temperature fluctuations decreased with the Richardson number in the outer region.

Hirota et al. (1997) measured velocity and temperature in a square duct using hot-wire probes for a single Reynolds number for fully turbulent flow under isothermal heating condition in the plane perpendicular to the flow. They observed that the turbulent heat fluxes in the streamwise direction are distorted towards the duct corner. They also found that the eddy diffusivity decreases and turbulent Prandtl number increases as approaching the duct corner. They also suggested that the influence of secondary flow on heat transport is weaker than that on the momentum transport. Ichimiya and Yamada (2005) numerically investigated the flow structure in a square duct for both thermally insulated walls and uniform temperature walls. They also studied the velocity field in a plane normal to the direction of the flow. Similar to Hirota et al. (1997), they observed that buoyancy influences the secondary flow development in the downstream direction.

In spite of several studies describing the flow structure above the heated wall, the question as to how the addition of heat affects the flow structure has not been well established to date. A direct comparison between the flow properties in the presence and absence of wall heating would provide a better insight into the impact of wall heating on the flow structure. In most of the previous studies however, the flow structure was investigated either in the absence of heat or presence of heat and no such comparison was made. Nicholl (1970) conducted such comparison for mean and turbulent intensity profiles; however, he did not observe any appreciable difference.

The present study is focused on the experimental investigation of the impact of wall heating on the flow structure in the near-wall region inside a channel. Special emphasis has been paid on the direct comparison of the flow characteristics at the same location and same inlet hydrodynamic conditions, in the presence and absence of wall heating. In addition, both laminar and turbulent flows were considered. This leads to a better insight into the physical mechanism(s) involved in this process for both flow regimes. A better knowledge of the influence of wall heating on the flow structure would help in improving the design and performance of thermal systems in particular, the heat exchangers.

2. Experimental setup

The experiments were conducted in a square channel with the inner cross-section of 7 cm × 7 cm. The channel consists of a 15 cm long settling chamber, 10 cm long trip section and 100 cm long test section. The settling chamber is made of aluminum and encompasses a honeycomb to straighten the flow before entering the trip section. A bleeder valve is installed at the top wall of the settling chamber to remove any trapped air locked in the channel. The

upstream end of the trip section is connected to the settling chamber by two Plexiglas flanges bolted together. The downstream end of the trip section is connected to the test section in the same manner. This allows the trip section to be easily removed. The trip section is a component used for other experiments. For the present experiments it is considered as a part of the channel. The trip and test section are made in the same fashion. The top and two side walls are made of ½ in thick non-tempered glass and the bottom wall is made of ½ in thick aluminum plate. The surface of the aluminum plate of the test section was coated black with a marker to minimize the reflection of the laser. The roughness of the aluminum plate is 0.56 μm which was measured using Surftest SJ-301 (Mitutoyo), which measures the surface height with the accuracy of 0.01 μm. The glass walls and aluminum plates of the channel were joined together by a clear silicone (Mastercraft 67-0859-0). The top edges between the glass walls were also reinforced with a layer of epoxy (Loctite D-609) because this edge is most susceptible to leaks. An aluminum end plate with an outlet valve is attached at the downstream end of the test section. The settling chamber and the test section were both bolted onto 5 cm high and 1.3 cm thick aluminum support plates. For the settling chamber, the length of support plates was 7.5 cm and for the test section, 94 cm long support plates were used (see Fig. 1B). The reason for two sets of support plates as oppose to just one pair was to ensure access to the bolts of the flanges that are connected between the trip section and both the settling chamber and the test section. These support plates are bolted to an exterior common base. A 750 W-240 V electric heater (Dimplex DBH-0750W) was placed immediately underneath the bottom plate of the test section in between the support plates. The heater was 72 cm long and was placed 15 cm from the upstream end of the test section (see Fig. 1B). The glass walls were not insulated in order to allow optical access to the flow for PIV measurements.

Clean tap water was used as the working fluid. A magnetic pump (Little Giant 58002 4MD series) was used to circulate water from a water tank through the channel in a closed loop. The pump was mounted on a separate wooden base. A rubber pad is inserted between the pump and the base to minimize vibrations. A valve downstream of the pump outlet (i.e. upstream of channel) was used to vary the flow rate to the channel. A ½ inch diameter tube connected this valve and the channel inlet. The outlet valve

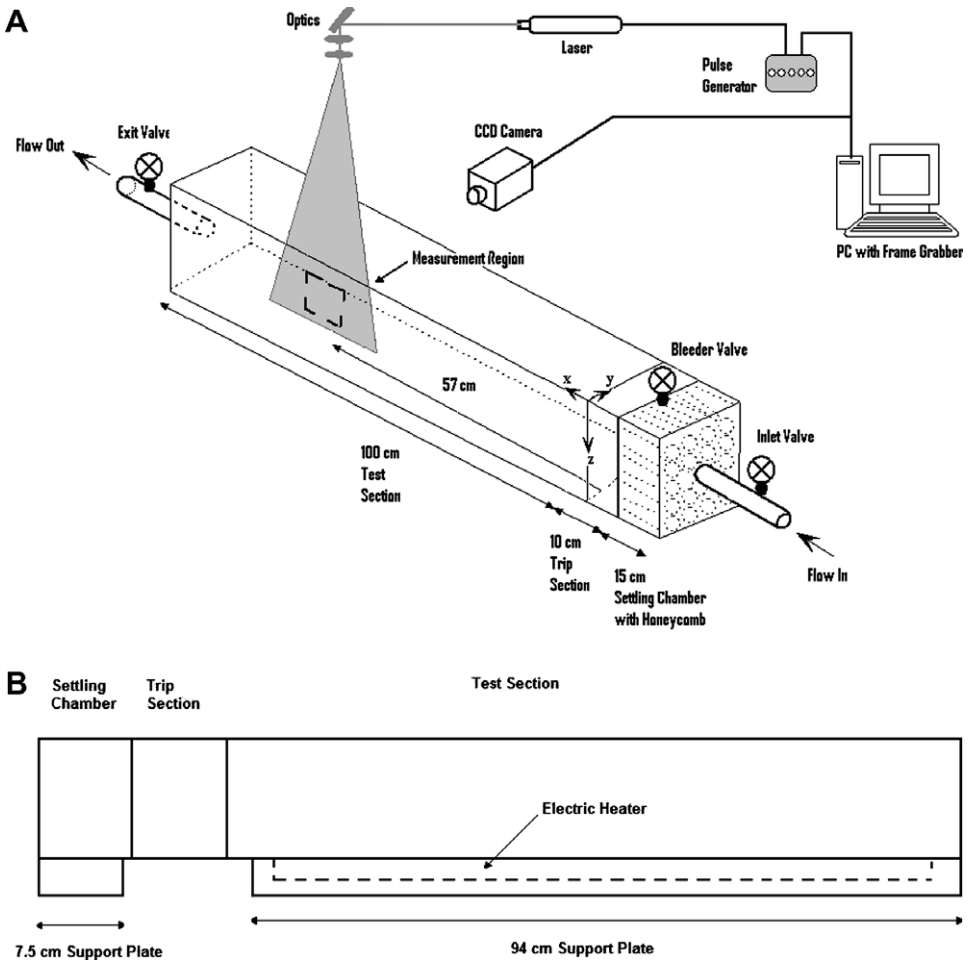

Fig. 1. (A) Schematic of the experimental setup (not to scale). The dashed lines show the measurement region, i.e. 3.2 cm horizontal and 2.4 cm vertical, (B) two-dimensional view of the square channel (not to scale). The dashed lines represent the electric heater.

that is located downstream of the channel was also connected to the water tank via a ½ inch diameter tube. Four experimental runs were considered that correspond to the mass flow rates of 0.035, 0.043, 0.258 and 0.277 kg/s. Hereinafter, case I refers to 0.035 kg/s, case II to 0.043 kg/s, case III refers to 0.258 kg/s and case IV to 0.277 kg/s. For each mass flow rate two cases were studied, one with the aluminum plate of the test section unheated, and the other with the aluminum plate of the test section heated. Since with the addition of heat, the volumetric flow rate changes due to the change in density and Reynolds number changes due to the change in density and viscosity, the mass flow rate is considered as the reference parameter for each case for both heated and unheated conditions.

The two-dimensional velocity fields were measured using particle image velocimetry (PIV). The measurements were made in a plane parallel to the side walls along the centerline of the channel at a distance of 57 cm from the upstream edge of the test section as shown in Fig. 1A. A Continuum Minilite 25 mJ Nd:YAG laser was used as the light source of the PIV measurements. A CCD camera (JAI CV-M2) with the resolution of 1600 × 1200 pixels was used to image the flow. The camera was mounted in the horizontal position. That is, the images were acquired with the dimensions of 1600 pixels in horizontal and 1200 pixels in vertical, with respect to the flow field. Since the present study is focused on investigating the impact of wall heating on the flow structure in the near-wall region, the measurement region was set close to the wall in order to obtain high-resolution velocity measurements in this region. The field of view of the camera was set equal to 3.2 cm horizontal and 2.4 cm vertical. The horizontal position of the camera was set in a way that the lower edge of the image coincides with the upper side of the aluminum wall. The camera was connected to a PC equipped with a frame grabber (DVR Express, IO Industries, London, ON, Canada) that acquires 8-bit images at a rate of 30 Hz. The water was seeded with silver-coated glass spheres, with the mean diameter of 15 μm (Potter Industries, Paoli, PA). These glass spheres were used as the tracer particles for the PIV measurements. A four-channel digital delay generator (555-4C, Berkeley Nucleonics Corporation, San Rafael CA) was used to control the timing of the laser light pulses. For each experimental run (i.e. for each heated and unheated case at a given mass flow rate), 3000 images were acquired at a rate of 30 Hz. That is, 1500 instantaneous velocity fields were obtained at a rate of 15 Hz. For the unheated cases, the data acquisition began 10 min after the start of flow to reach steady state. For the heated cases, the data acquisition was started 90 min after the heater was turned on at a given mass flow rate.

The PIV technique computes velocity vectors by cross-correlating the interrogation region in the first image with the corresponding search region in the second image of an image pair. In the present study, the size of the interrogation region was set equal to 32 × 32 pixels and the size of the search region was set equal to 64 × 64 pixels. A 50% window overlap was used in order to increase the nominal resolution of the velocity field to 16 × 16 pixels. This resulted in the spatial resolution of 0.34 × 0.34 mm of the velocity field. Due to the difference in the velocity magnitudes for all cases, a constant time separation between the two images of an image pair will give different particle shifts for different cases. That is, when the velocity magnitude is small the particle shift will be smaller. Very small particle shift increases the uncertainty in the velocity measurements. Thus, the time separation between the two images of an image pair was varied in each case, in order to obtain reasonable particle shifts. The time separation, dt, between two images of an image pair for different cases are tabulated in Table 1. A scheme was used to identify the spurious velocity vectors and then correct them using a local median test (Siddiqui et al., 2001). Typically, 1% of the velocity vectors were spurious. The uncertainty in velocity measurements for each case is also presented in Table 1.

The temperature at the surface of the bottom plate and in the near-wall region was measured in a separate set of experiments for heated cases under identical conditions. A rake of eight T-type thermocouples with an accuracy of 0.1 °C was placed 60 cm from the upstream end of the test section. The thermocouples were spaced 2 mm apart vertically with the first thermocouple located on the surface of the bottom wall. The temperature data was acquired via a 16-channel data acquisition card (PCI-6036E, National Instruments) using the LabView data acquisition software.

Table 1
Parameters for different cases

Case		I	II	III	IV
Mass flow rate (kg/s)		0.035	0.043	0.258	0.277
Wall temperature (°C)		32.6	31.2	29.7	29.9
Richardson number		−0.4684	−0.2773	−0.003	−0.001
Rayleigh number		3.37×10^8	3.18×10^8	1.63×10^8	1.41×10^8
dt (ms)	Unheated	25	10	4	3
	Heated	20	8	4	3
Uncertainty in velocity measurements (%)	Unheated	4.14	6.43	2.86	2.96
	Heated	4.39	6.71	3.08	3.34
Friction velocity (cm/s)	Unheated	0. 100	0.094	0.280	0.318
	Heated	0.133	0.176	0.300	0.327

A signal conditioner (SCXI-1102, National Instruments) was used to amplify the signal before passing through the data acquisition card. The data were acquired for 10 min at a rate of 100 Hz. The thermocouples were calibrated before and after the experiments using Traceable Digital Thermometer (Control Company, USA) which has resolution of 0.001 °C with ±0.05 °C accuracy. The calibration was conducted in a large water tank where the water depth was 26 cm. Both the thermocouple and digital thermometer were placed side by side in the middle at a depth of 12 cm. The average temperature of the bottom plate for the heated runs at all flow rates are also listed in Table 1.

3. Results

To check whether the flow was developed at the measurement location, the time-averaged streamwise velocity profiles near the upstream and downstream ends of the camera field of view (3.2 cm apart) were compared for all cases. The mean velocity profiles at both locations are plotted in Fig. 2 for all cases. In the present study, the depth, z, is referenced from the inner surface of the bottom wall. That is, $z = 0$ is at the wall with the positive z-axis pointing upward towards the middle of the channel. The plot shows that overall the profiles at both locations overlap well for all cases with some minor deviations at certain depth for few cases. The average difference between the two velocity profiles was less than 5% for all cases except for the heated profile of case I where the difference was 6.7%. Considering the uncertainty in the velocity measurements, these differences were relatively small and thus, it was concluded that for all cases, the flow was developed.

Fig. 3A shows the vertical profiles of the mean streamwise velocity. The mean streamwise velocity was computed by averaging the velocity data at each depth temporally and spatially. That is, for each experimental run, the time series were extracted at each grid point. The average velocity was obtained at each grid point by time-averaging. The time-averaged velocities at all grid points at a particular depth were then spatially averaged. This provided the spatial-temporal averaged velocity at each depth. The plot in Fig. 3A shows that the mean streamwise velocity component for the unheated condition is greater than that for the heated condition for cases III and IV. The plot also shows that within the measurement region, the streamwise velocity was reduced on average by 15% for case IV and 13% for case III when heat was added from the bottom plate. However, the opposite trend is observed for the two lower flow rates (cases I and II). That is, when heat was added, the mean streamwise velocity at these flow rates was increased by a factor of more than 2.5 in the close vicinity of the wall. However, as the distance from the wall

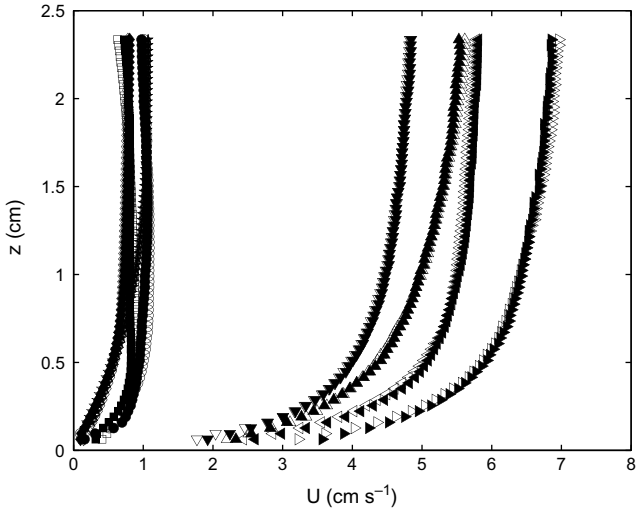

Fig. 2. Vertical profiles of the mean streamwise velocity for heated and unheated conditions at the upstream and downstream ends of the field of view (3.2 cm apart). Case I unheated (◇), Case I heated (□), Case II unheated (pentagram), Case II heated (○), Case III unheated (▲), Case III heated (▼), Case IV unheated (►) and Case IV heated (◄). Open symbols: upstream end; solid symbols: downstream end.

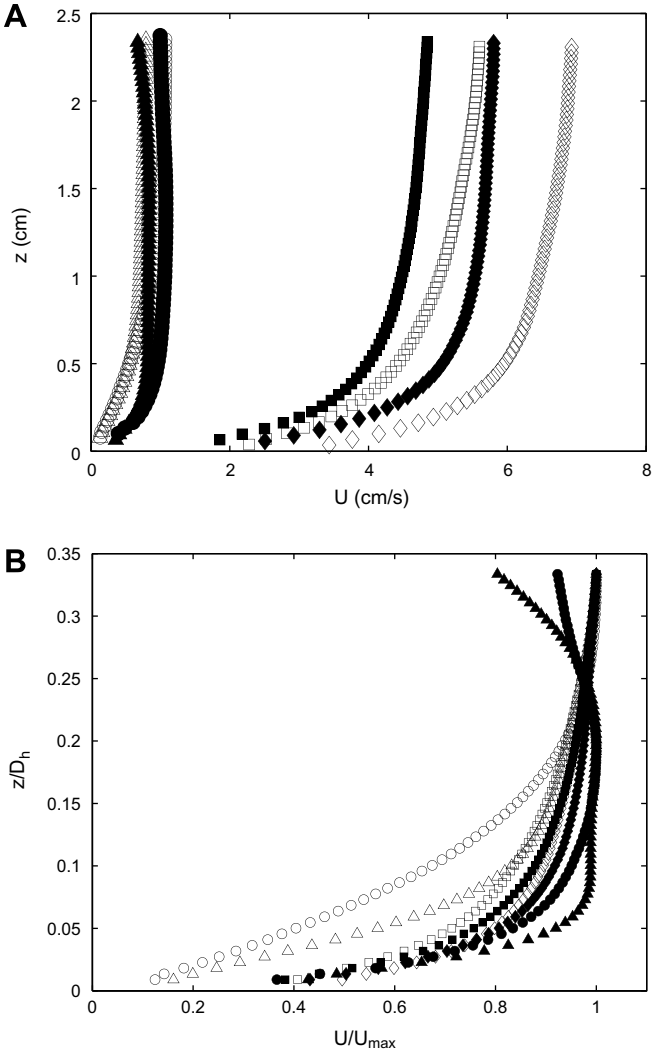

Fig. 3. Vertical profiles of the mean streamwise velocity in (A) dimensional form, (B) non-dimensional form. Case I (Δ), Case II (○), Case III (□) and Case IV (◇). Open symbols: unheated condition; solid symbols: heated condition. D_h is the hydraulic diameter of the channel.

increased, the magnitude of the streamwise velocity became almost constant for some distance and then started to decrease. It was also observed that at a distance of 1.8–2 cm from the wall, the velocity magnitudes for both heated and unheated cases became equal and further away from the wall, the velocity magnitude for unheated case become greater than the heat case. The plot in Fig. 3A also indicates that the change in velocity for different cases between heated and unheated conditions is not the same. This is due to the reason that the fluid temperature evolved differently in all four heated cases. This can be explained as follows. As will be discussed later, the turbulence production and its interaction with the buoyancy forces varied for different flow rates under the heated condition. Thus, the heat transfer coefficient is also expected to vary from case to case. That is, the difference in heat transfer coefficients for heated and unheated conditions must be varied in all four cases. In the present study, the wall heat flux was constant, thus, due to the difference in the heat transfer coefficient, the fluid temperature varied from case to case.

The crossing of the velocity profiles for heated and unheated cases at a certain distance from the wall can be explained as follows. At a given condition, the mass flow rate of water was the same. For cases I and II, the average velocity in the near-wall region for heated condition was more than a factor of 2.5 larger than that for the unheated condition. The percentage decrease in the density due to heating was significantly lower than the percentage increase in the velocity. Thus, in the near-wall region, the mass flux for heated condition was greater than that for the unheated condition. To satisfy continuity, the mass flux of water for heated case must be decreased in some other region. Thus, the decrease in the streamwise velocity magnitude away from the wall for the heat case is to satisfy mass conservation. The same physical argument is also applicable to the higher flow rates (i.e. cases III and IV). In these cases it was observed that the mass flux in the near-wall region for the heated condition is lower than the unheated condition, therefore, it is expected that in a region away from the wall (outside the measurement region), the streamwise velocity magnitude for the heated case would be greater than that for the unheated case.

The mean velocity normalized by the maximum velocity within the measurement region, is plotted versus the normalized depth in Fig. 3B for all cases. The plot shows that for cases III and IV, the profiles collapsed quite well for both heated and unheated cases indicating that for the turbulent regime in the near-wall region, the mean velocity behavior is not significantly influenced by the wall heating. For cases I and II, the profiles deviated for heated and unheated conditions. This indicates that wall heating influences the mean velocity behavior in the near-wall region for these two cases. The most significant influence was observed at the lowest flow rate (i.e. case I with heating condition) where the mean velocity was almost uniform in the region $0.08 < z/D_h < 0.22$, which is followed by a decrease in the mean velocity towards the channel core. The typical boundary layer trend for heated condition started to recover with an increase in the mass flow rate.

As mentioned in the experimental setup section, the electric heater was placed under the test section downstream of the trip section. Thus, for the heated cases, the trip section acts as an unheated starting length. Ameel (1997) showed that the average Nusselt number and the average plate temperature are more affected by an unheated starting length when the flow is laminar. As shown later, for unheated condition, cases I and II were in the laminar regime. Thus, it is expected that the properties at these two cases for heated condition would be more affected by the unheated starting length compared to cases III and IV.

The friction velocity was computed using the relation

$$u_* = \sqrt{\nu \frac{\mathrm{d}U}{\mathrm{d}z}}, \tag{1}$$

where, $\frac{\mathrm{d}U}{\mathrm{d}z}$ is the mean streamwise velocity gradient at the wall and ν is the kinematic viscosity. The mean streamwise velocity gradient was computed between the velocity data nearest to the wall and the velocity at the wall, where the latter is taken as zero due to the no slip condition. The values of the friction velocity for both heated and unheated conditions are presented in Table 1 for all cases. For the accurate estimation of the friction velocity, the nearest velocity measurement location must be within the viscous sublayer, that is, $y^+ < 10$. In the present study, the nearest velocity measurement with respect to the bottom wall was located at a height of 0.672 mm from the wall. For case IV, where the friction velocity was the largest, at this nearest velocity location, $y^+ = 2.4$. For other three cases, the values of y^+ are even smaller than 2.4. Thus, the friction velocity is accurately computed. At a given mass flow rate, the comparison of the friction velocities for heated and unheated conditions shows that for cases III and IV, the friction velocity remained almost the same when heat was added from bottom, whereas, for cases I and II, the friction velocity was increased with the heat addition.

The PIV measurements provide instantaneous velocity fields. The turbulent velocity fields were computed by subtracting the time-averaged mean velocity at each grid point, from the corresponding instantaneous velocity. From the turbulent velocity fields, a number of turbulent characteristics were computed. The profiles of the root-mean-square (RMS) horizontal turbulent velocity component are plotted in dimensional and non-dimensional forms in Fig. 4A and B, respectively. The profiles show that the magnitude of the horizontal turbulent velocity is larger for the unheated condition for cases III and IV, whereas, the opposite trend (similar to Fig. 3) is observed for cases I and II. That is, the horizontal turbulent velocity is larger for the heated condition. The plot also shows that for unheated condition, the magnitudes of the turbulent velocity for cases I and II are very small except in the near-wall region. This indicates that for these two cases the flow is almost laminar. However, at the same flow rates, when

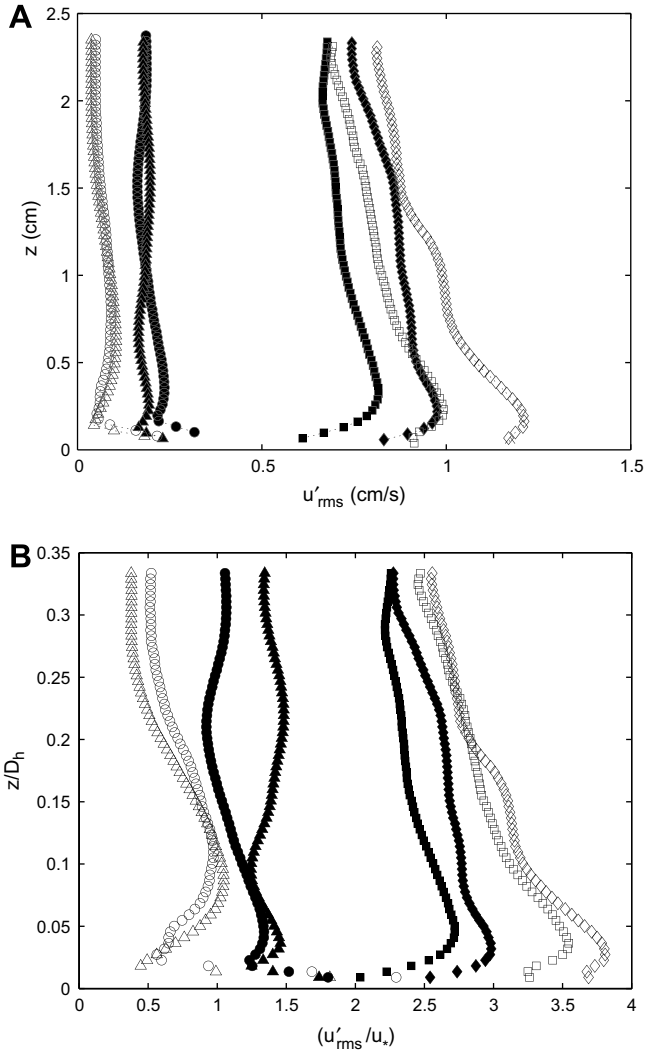

Fig. 4. RMS horizontal turbulent velocity versus the height from the wall in (A) dimensional form, (B) non-dimensional form. Case I (Δ), Case II (○), Case III (□) and Case IV (◇). Open symbols: unheated condition; solid symbols: heated condition.

heat is supplied, the turbulent intensity increased. For cases III and IV, the turbulent intensity was decreased with the heat addition. Furthermore, for cases III and IV under both conditions, the horizontal turbulent intensity increased with the distance from the wall up to approximately 3 mm ($z/D_h \approx 0.04$) and then started to decrease towards the centerline. The maximum turbulent intensity was observed approximately at the same distance from the wall for both heated and unheated conditions. With the heat addition, the horizontal turbulent velocity decreased by approximately 25% within the 3 mm depth and by approximately 10% in the region away from the wall for cases III and IV. For cases I and II at both heated and unheated conditions, the maximum horizontal turbulent intensity was observed in the close vicinity of the wall which decreased sharply up to a distance of 1.5 mm ($z/D_h \approx 0.02$) from the wall. As the distance further increased, some variations are observed in the turbulent horizontal intensity, however, at heights $z/D_h > 0.25$, the turbulent horizontal intensity became approximately constant. The comparison between heated and unheated conditions shows that with the heat addition, the horizontal turbulent intensity for cases I and II was increased by approximately a factor of two. The plot in Fig. 3B also shows that for both heated and unheated conditions, the profiles for cases I and II, and cases III and IV formed distinct groups. For unheated condition, the distinct grouping is due to the reason that cases I and II correspond to almost laminar regime, whereas, cases III and IV correspond to the fully turbulent regime. The distinct grouping for heated condition indicates that the impact of wall heating on the initially laminar and turbulent flows is different. This issue will be discussed later in detail.

The profiles of the RMS vertical turbulent velocity are shown in Fig. 5A and B in dimensional and non-dimensional forms, respectively. The impact of heat addition

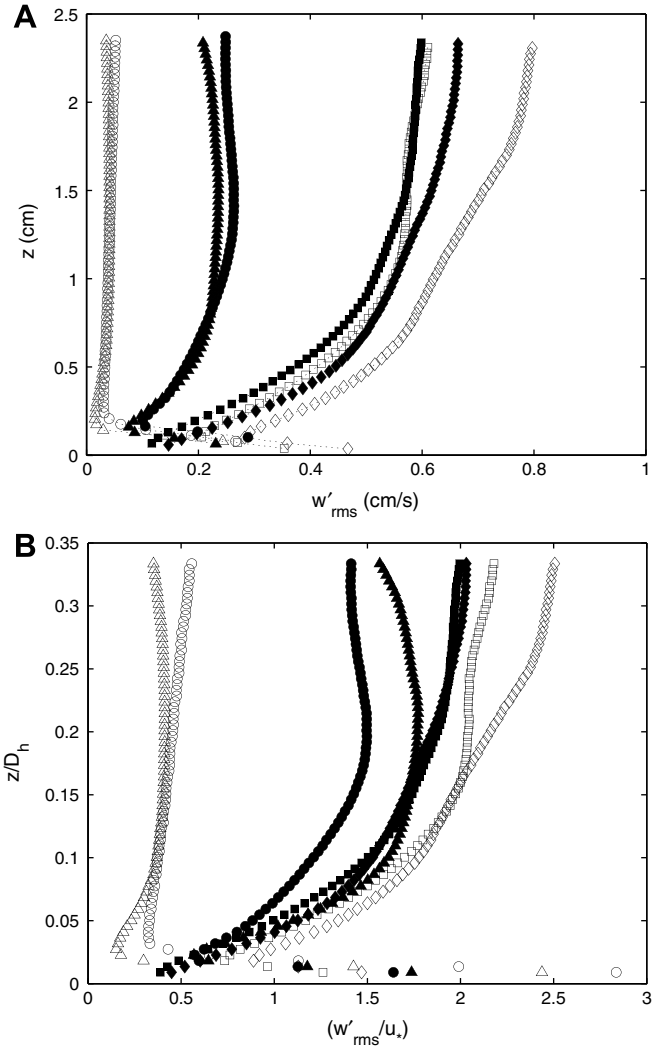

Fig. 5. RMS vertical turbulent velocity versus the height from the wall in (A) dimensional form, (B) non-dimensional form. Case I (Δ), Case II (○), Case III (□) and Case IV (◇). Open symbols: unheated condition; solid symbols: heated condition.

for different cases was similar to that observed for the horizontal turbulent velocity. That is, for cases III and IV, the magnitude of the vertical turbulent velocity decreased with the heat addition, whereas, for cases I and II, the magnitude of the vertical turbulent velocity increased with the heat addition. The variation in the vertical turbulent velocity with the distance from the wall is similar for all cases. That is, the vertical turbulent velocity first decreased sharply with the distance from the wall up to $z/D_h \approx 0.02$ and then increased at greater heights, except for the unheated condition for cases I and II where it stays almost constant with very small magnitude. As mentioned earlier, this could be due to the reason that the flow was in the laminar regime for these two cases. For cases I and II in the region away from the wall, the vertical turbulent velocity was increased by almost a factor of five with the heat addition. This indicates that the flow that was in the laminar regime before heat addition became turbulent when heat was added.

The non-dimensional plots in Fig. 5B shows distinct grouping similar to that in Fig. 4B for the unheated condition, which is due to the laminar and turbulent flow regimes for, cases I and II and III and IV, as mentioned earlier. For heated condition, the plot shows that in the region ($z/D_h < 0.2$), all profiles except for case II collapsed well. As the distance further increases, the profile of case I started to deviate. The results indicate that for the flow that was initially turbulent (cases III and IV), the impact of wall heating on the vertical turbulent intensity is similar. However, for the flow that is initially laminar (cases I and II), the impact of wall heating is different.

The turbulent kinetic energy was computed using the relation

$$E_K = \frac{1}{2}u'^2 + w'^2, \tag{2}$$

where the turbulent cross-stream component of velocity (v'^2) was assumed to be equal to the vertical velocity component. The vertical profiles of the turbulent kinetic energy are plotted in Fig. 6A and B in dimensional and non-dimensional forms, respectively. As the results in Figs. 4 and 5 show that the magnitude of the horizontal turbulent velocity is higher than the vertical turbulent velocity in the near-wall region, the shape of the turbulent kinetic energy profiles in this region is similar to that of the horizontal turbulent velocity. In the outer region, the horizontal velocity decreases and the vertical velocity increases, with comparable magnitudes, which resulted in the almost constant turbulent kinetic energy in the outer region. The comparison between the profiles for heated and unheated conditions shows that when heat is added, the turbulent kinetic energy is decreased for cases III and IV, and increased for cases I and II. The non-dimensional plot in Fig. 6B shows similar profile grouping as in Figs. 4 and 5. The results in Figs. 4–6 also show that for the heated condition, the non-dimensional magnitude of turbulent intensities for case I is larger than case II. These issues will be discussed later in the discussion section.

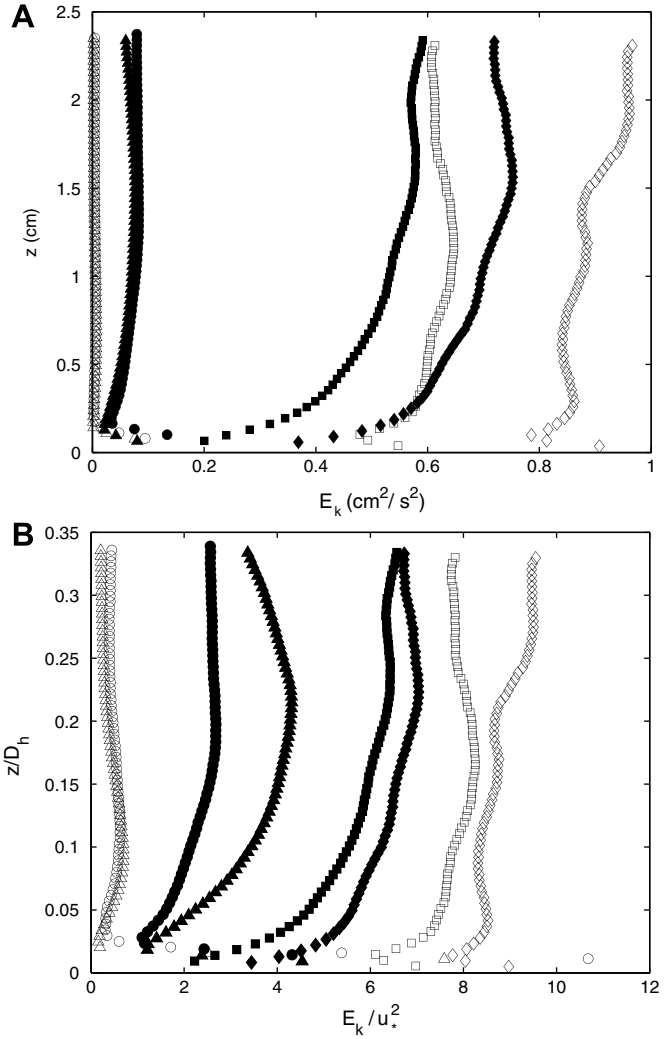

Fig. 6. Turbulent kinetic energy is plotted versus the height from the wall in (A) dimensional form, (B) non-dimensional form. Case I (Δ), Case II (○), Case III (□) and Case IV (◇). Open symbols: unheated condition; solid symbols: heated condition.

The Reynolds stress ($-\overline{u'w'}$) profiles are presented in Fig. 7A and B as a function of depth in the dimensional and non-dimensional forms, respectively. The results show that for cases III and IV, the profiles for both heated and unheated conditions show the classical behavior. That is, the Reynolds stress increased with the distance in the near-wall region to a peak value and then decreased towards the outer region. The plot also shows that at these Reynolds numbers, the magnitude of the Reynolds stress is higher for the unheated condition. For cases I and II, a different trend is observed. For the unheated condition, the Reynolds stress is almost zero, confirming that the flow was in the laminar regime at these two flow rates in the absence of heat (Fig. 7A). When heat was added at these flow rates, the Reynolds stress profiles showed the classical trend up to a distance of 1 cm ($z/D_h \approx 0.14$) from the wall and then the Reynolds stress became negative while its magnitude increased with distance up to $z = 2$

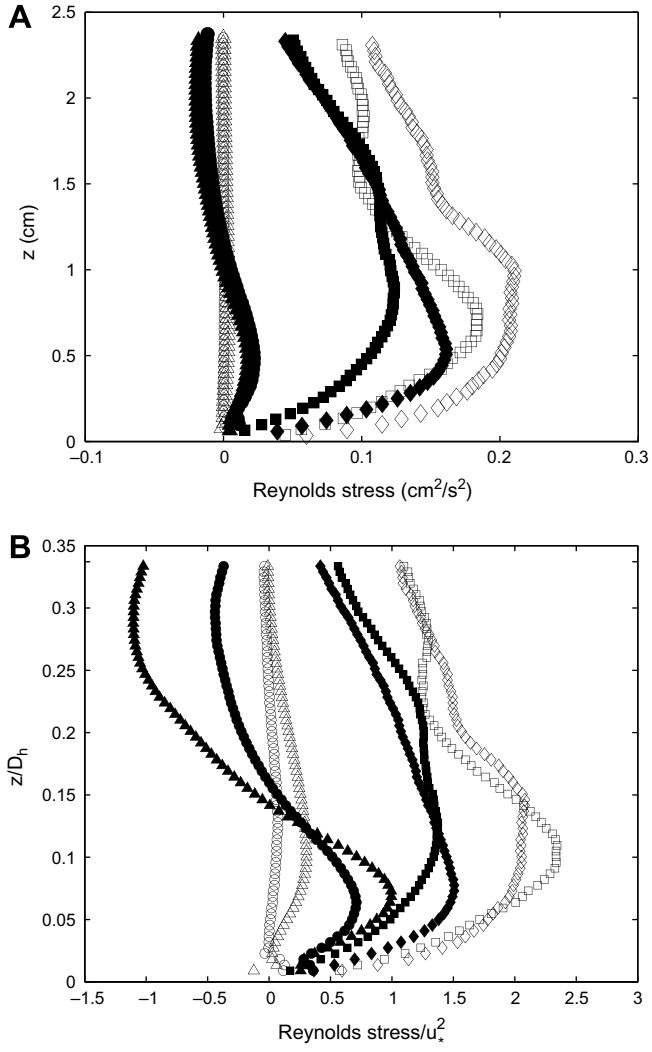

Fig. 7. Vertical profiles of the Reynolds Stress in (A) dimensional form, (B) non-dimensional form. Case I (Δ), Case II (○), Case III (□) and Case IV (◇). Open symbols: unheated condition; solid symbols: heated condition.

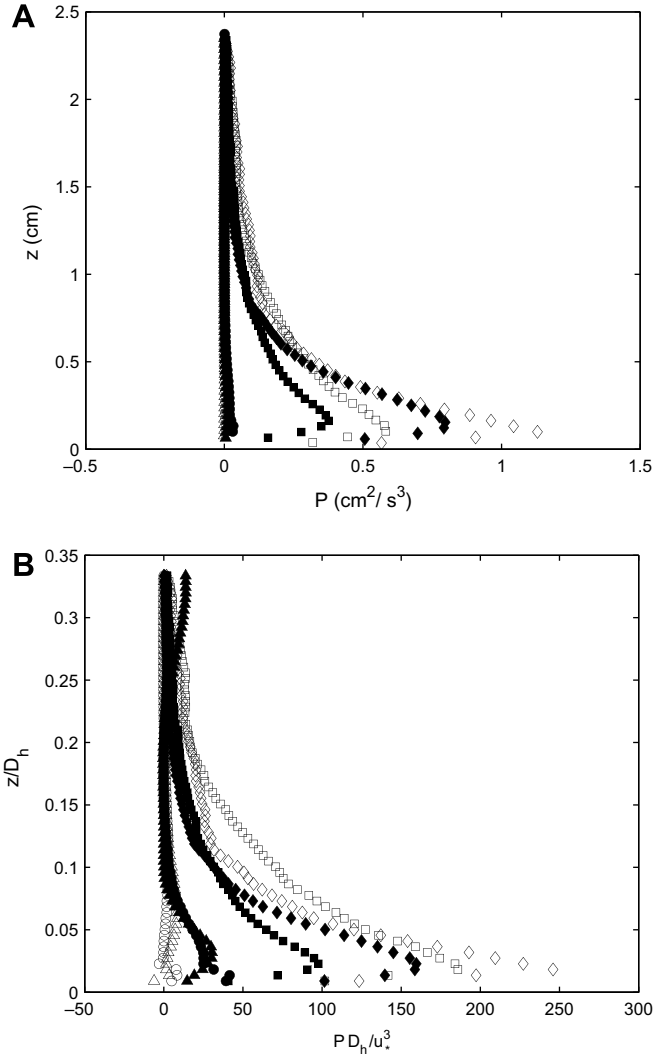

Fig. 8. Vertical profiles of the rate of turbulent kinetic energy production in (A) dimensional form, (B) non-dimensional form. Case I (Δ), Case II (○), Case III (□) and Case IV (◇). Open symbols: unheated condition; solid symbols: heated condition.

cm ($z/D_h \approx 0.3$) after which it began to decrease. The normalized plot (Fig. 7B) shows that for heated condition, the non-dimensional magnitude of Reynolds stress for cases III and IV is similar, however, for the two lower flow rate cases, the non-dimensional magnitude of Reynolds stress for case I is larger that case II.

The turbulent kinetic energy production due to the mean shear can be computed using the relation

$$P = -\overline{u'w'}\frac{\mathrm{d}U}{\mathrm{d}z}, \tag{3}$$

where $-\overline{u'w'}$ is the Reynolds stress and $\frac{\mathrm{d}U}{\mathrm{d}z}$ is the mean streamwise velocity gradient. The vertical profiles of the turbulent kinetic energy production are plotted in Fig. 8A and B as a function of depth in dimensional and non-dimensional forms, respectively. The overall trend in the production profiles is similar to the classical profiles of wall bounded flows. That is, the turbulent energy production increased very sharply from zero to a peak value in the near-wall region and then decreased towards the outer region. As mentioned earlier, for unheated condition at the two lower flow rates (cases I and II), the flow was in the laminar regime. The results in Fig. 8 further confirm this by showing that the energy production is almost zero for these two cases. The plot in Fig. 8B also shows that for case II heated condition, the energy production is also almost zero at heights $z/D_h > 0.08$, whereas, for case I, the energy production again started to increase at heights $z/D_h > 0.25$. The Reynolds stress profiles for these cases in Fig. 7 showed negative Reynolds stress at heights $z/D_h > 0.14$. Thus, we expect negative production in this region. However, the mean velocity gradients for cases I and II are almost zero in the region $0.14 < z/D_h < 0.25$ and negative for $z/D_h > 0.25$ (see Fig. 3). This resulted in positive energy production in this region. Due to the large magnitudes of mean velocity gradients and Reynolds stress for case I in this region compared to case II, the positive energy

production of case I is prominent in Fig. 8B. The results in Figs. 4–6 indicate that for cases I and II when heat is added, the turbulent intensities are significantly enhanced compared to the unheated condition over the entire measurement plane. The results in Fig. 8 however, indicate that for cases I and II, the energy production due to the mean shear for the heated condition is very small and mainly restricted to small region. This implies that the turbulence due to the mean shear is negligible and the turbulence is primarily generated by the buoyancy flux. Thus, it can be concluded that in channel flows which are initially laminar in the absence of heat transfer, when heat is supplied to create unstably stratified regime, the turbulence generation is almost entirely due to the buoyancy flux.

For cases III and IV, the plots show that the energy production is higher for the unheated condition compared to the heated one. This is due to the higher magnitudes of the Reynolds stress for the unheated condition and almost comparable magnitudes of the mean velocity gradients for both conditions. The plots show that for these cases, the maximum energy production is reduced by approximately 30% when heat is added to the flow.

PIV velocity fields provide four velocity gradients in a plane. Doron et al. (2001) compared five different methods of estimating the energy dissipation, and showed that the "direct" method that uses velocity gradients computed from the two-dimensional turbulent velocity field obtained from PIV measurements was the most accurate. The rate of turbulent kinetic energy dissipation was computed using the direct method with the equation

$$\varepsilon = 3\nu\left[\overline{\left(\frac{\partial u'}{\partial x}\right)^2} + \overline{\left(\frac{\partial w'}{\partial z}\right)^2} + \overline{\left(\frac{\partial u'}{\partial z}\right)^2} + \overline{\left(\frac{\partial w'}{\partial x}\right)^2} + 2\overline{\left(\frac{\partial u'}{\partial z}\frac{\partial w'}{\partial x}\right)} + \frac{2}{3}\overline{\left(\frac{\partial u'}{\partial x}\frac{\partial w'}{\partial z}\right)}\right], \quad (4)$$

where $\frac{\partial u'}{\partial x}$ is the streamwise velocity gradient in the horizontal direction, $\frac{\partial u'}{\partial z}$ is the streamwise velocity gradient in the vertical direction, $\frac{\partial w'}{\partial x}$ is the vertical velocity gradient in the horizontal direction and $\frac{\partial w'}{\partial z}$ is the vertical velocity gradient in the vertical direction. The overbar denotes time averaging. The rate of energy dissipation is plotted in Fig. 9A and B as a function of depth in dimensional and non-dimensional forms, respectively. The plot shows that the rate of energy dissipation is largest adjacent to the wall, which decreased with the distance from the wall and became almost constant in the outer region. In dimensional form for cases I and II, the dissipation is almost negligible expect near the wall, where the dissipation rate for the heated condition is higher than the unheated one. For cases III and IV, the plot shows that the dissipation rate is higher for the unheated condition. In non-dimensional form (Fig. 9B), the plot shows that the dissipation rates for cases II–IV have comparable magnitude, which is almost a factor of three smaller for the heated condition. For case I, the dissipation magnitude is smaller with almost negligible values for the unheated condition. When computing the dissipation rate from PIV velocity gradients, it is important to know whether the PIV measurements have enough spatial resolution to capture majority of the dissipation. The smallest spatial scale that was resolved by the given PIV measurements was 0.672 mm, corresponding to a wavenumber, $k = 9350$ rad m^{-1}, Kolmogorov length scale, $\eta = 263$ μm, and thus, $k\eta = 2.46$. Tennekes and Lumley (1972) have shown that the maximum dissipation occurs around $k\eta = 0.2$. They have also shown that almost the entire dissipation takes place for $k\eta < 5$. Based on the results in Tennekes and Lumley (1972), the given PIV measurements resolve more than 90% of the total dissipation.

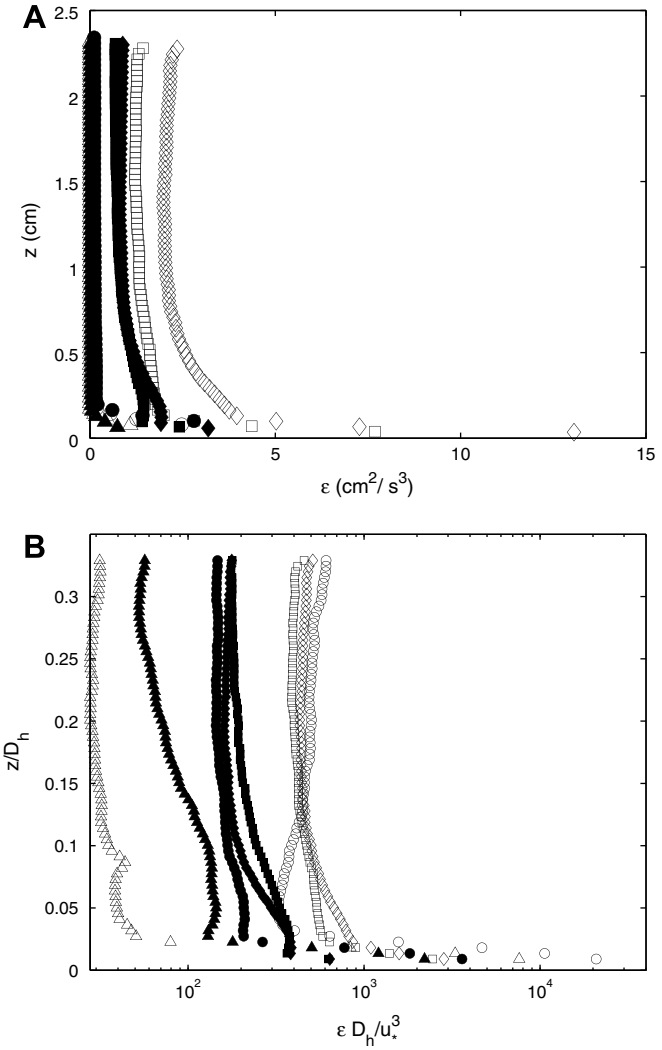

Fig. 9. Vertical profiles of the rate of turbulent kinetic energy dissipation in (A) dimensional form, (B) non-dimensional form. Case I (Δ), Case II (○), Case III (□) and Case IV (◇). Open symbols: unheated condition; solid symbols: heated condition.

4. Discussion

Results in the previous section show that when a flow is unstably stratified via heating through a bottom wall, both

the mean and turbulent characteristics are affected. We have considered four cases, two of which correspond to the laminar regime in the absence of heat (cases I and II) and the other two correspond to the turbulent regime (cases III and IV). The results have shown that the impact of wall heating on the flow behavior is significantly different for the laminar and turbulent flows. It was found that when a flow that is originally laminar is heated, the mean streamwise velocity in the near-wall region is significantly increased and turbulence is generated in the flow. Thus, a flow that is originally laminar becomes turbulent with the heat addition. However, when the flow is in the turbulent regime, addition of heat reduces the magnitudes of mean streamwise velocity and turbulent properties.

For the heated cases in the present study, there are two mechanisms of turbulence production, one is the mean shear and the other is the buoyancy flux. The relative magnitudes of the turbulence production due to the buoyancy and mean shear is quantified in terms of the gradient Richardson number (R_i) which is defined as

$$R_i = -g\frac{\partial\rho}{\partial z}/\rho\left(\frac{\partial U}{\partial z}\right)^2, \tag{5}$$

where $\partial\rho/\partial z$ is the vertical density gradient and g is the acceleration due to gravity (Turner, 1973). When $R_i < 0$, the flow becomes thermally unstable. As mentioned in the experimental setup section, the temperature was measured in the near-wall region in a separate set of experiments under the identical conditions. The values of R_i were computed from the temperature data. The values of R_i in the near-wall region for all heated cases are presented in Table 1. The results show that the magnitude of the Richardson number is largest for case I and decreased monotonically to case IV. This indicates that the turbulence production due to buoyancy is more dominant at the lower flow rates compared to the higher flow rates. When the flow is unheated, the only source of turbulence is the mean shear. The results show that for unheated condition at low flow rates, the turbulent intensities are almost negligible and the turbulence production due to the mean shear is almost zero. This indicates that in the absence of heat transfer, the flow is in the laminar regime. When heat is applied, the magnitude of turbulent intensities increased drastically, however, the magnitude of the turbulent kinetic energy production due to the mean shear remained close to zero. This implies that the strong turbulent intensities observed for these cases are due to the turbulence production by buoyancy. Turner (1973) argued that for thermally stratified flows, the Reynolds number for the transition to turbulence depends on the Richardson number. The present results confirm this argument by showing that a flow in the laminar regime could become turbulent at relatively low Reynolds number when unstable thermal stratification is introduced. In the present study however, we are not able to estimate the critical Richardson number for the transition.

In the turbulent regime (i.e. cases III and IV), the Richardson number is several orders of magnitude lower than that for cases I and II. This indicates that the impact of buoyancy on turbulence production is relatively small and mean shear is the dominant mechanism of turbulence production. The results show that in this regime, the magnitude of the turbulent characteristics decreased when heat is added. This trend is opposite to that observed for initially laminar flows. Turner (1973) argued that in stratified fully developed turbulent flows where the Richardson number is small, the turbulent kinetic energy is systemically removed over a range of wavenumbers by working against buoyancy forces. He further argued that the energy production due to the mean shear is balanced by the rate of working against the buoyancy forces and the viscous dissipation. Townsend (1958) estimated the ratio of the total energy loss to energy production (due to the mean shear) in a stratified flow and plotted it versus the turbulent intensity for various buoyancy effects. The plot shows that the total energy loss to energy production ratio increases with an increase in the buoyancy effects. The plot also shows that for a given turbulent intensity, this ratio is always higher for the stratified flow compared to the unstratified flow, where in the latter case the energy loss is entirely due to viscous dissipation. This indicates that in a fully turbulent flow at a particular flow rate (i.e. case III or IV) when the flow become stratified, the turbulence work against the buoyancy forces resulting in a decrease in the turbulent intensities as observed in Figs. 4 and 5. A decrease in the turbulent intensities resulted in a decrease in Reynolds stress and thus, the energy production as seen in Figs. 7 and 8.

These results indicate that the effect of stratification on the flow structure is significantly different for the flow that is originally in the laminar regime compared to that in the turbulent regime. For the same flow rate, in the laminar regime, stratification leads to the transition to turbulent regime if the Richardson number is higher than certain critical value. However, in the turbulent regime, stratification leads to the decrease in turbulence level due to its work against the buoyancy forces. Furthermore, in unstratified flows the transition from laminar to turbulent regimes occurs with an increase in the Reynolds number and turbulence is produced by the mean shear. However, when a laminar flow becomes turbulent due to the stratification (in the same range of Reynolds number), the turbulence production due to the mean shear remains negligible and the turbulence is produced almost entirely due to buoyancy.

The mean velocity profiles in Fig. 3 also show a trend similar to that of the turbulent properties. That is, for cases I and II, the mean velocity is increased in the near-surface region when heat is added, whereas, for cases III and IV, the mean velocity is decreased with the addition of heat. One plausible explanation for this tend is that in the laminar regime where the Reynolds number is low, the viscous effects are relatively more significant than that in the turbulent regime where the Reynolds number is high. Thus, when heat is added, the viscosity of the fluid is reduced

which resulted in an increase in the mean velocity in the near-wall region. At higher Reynolds numbers in the fully turbulent regime where the viscous effects are insignificant, the decrease in viscosity has no significant impact on the mean velocity in the near-wall region. However, this reason cannot explain the trend of decrease in mean velocity with the heat addition. The reason for this trend is still under investigation. The mean velocity profiles for heated condition show that the effect of unstable stratification has different impact for cases I and II and cases III and IV (Fig. 3B). The instability in stratification is quantified in terms of the Richardson number (Fukui and Nakajima, 1985). Thus, the instability decreased monotonically from case I to case IV. For cases III and IV, the plot shows that the velocity decreases with an increase in instability. For cases I and II, the plot shows that near the wall, velocity increases with an increase in instability. Immediately adjacent to the wall in the region $z/D_h < 0.02$, the profiles at different instabilities collapsed which indicates that the instability influences the flow structure at a certain distance from wall. This behavior is consistent with Fukui and Nakajima (1985) who also observed that the mean velocity profiles at different instabilities collapsed immediately adjacent to the wall and dispersed at greater heights.

The normalized horizontal turbulent intensity profiles for heated condition (Fig. 4B) also show that the impact of instability is different for cases I and II and cases III and IV. For cases I and II where the flow was originally laminar, the horizontal turbulent intensity increased with an increase in instability, whereas for cases III and IV where the flow was originally turbulent, the horizontal turbulent intensity decreased with an increase in instability. The normalized vertical intensity profiles for heated condition (Fig. 5B) show the same trend for cases I and II, however, for cases III and IV, the profiles show no significant effect of instability. The effect of instability on the overall turbulent intensities is depicted in the normalized plots of turbulent kinetic energy (Fig. 6B). The profiles show the trend similar to that in Fig. 4B, i.e. the turbulent kinetic energy increased with instability for cases I and II and decreased with instability for cases III and IV. This behavior can be explained as follows. As discussed earlier, the buoyancy or unstable stratification is the mechanism of turbulence generation in the originally laminar flows. Therefore, higher the magnitude of instability, more buoyancy-driven turbulence is expected to generate. For originally turbulent flows, the turbulence works against the buoyancy forces. Thus, higher the magnitude of instability, more work is performed against buoyancy forces, causing a decrease in the turbulent kinetic energy. Fukui and Nakajima (1985) also studied the effect of instability in stratification on turbulent intensities for fully turbulent flows. They observed an increase in normalized horizontal turbulent velocity with instability in the inner region, and no variation at greater heights. For the normalized vertical turbulent velocity, they found that the vertical velocity decreased with instability in the inner region, and increased with instability at greater heights. Their trend for the horizontal turbulent velocity was different from the present study; however, the trend of vertical turbulent velocity in the inner region is consistent with the present study. Furthermore, in the near-wall region, they observed that the vertical turbulent velocity is less sensitive to the instability than the horizontal turbulent velocity, which is also in agreement with the present study.

The Reynolds stress profiles in Fig. 7B showed that for cases I and II, the magnitude of Reynolds stress increased with an increase in instability. For cases III and IV, the Reynolds stress decreased with an increase in instability in the near-wall region, and slightly increased with instability in the outer region. The production profiles (Fig. 8B) showed that for cases III and IV, the energy production decreased with an increase in instability, whereas, for cases I and II, the instability has no significant effect on the energy production. This is due to the reason that the instability in stratification for originally laminar flow has no significant contribution to the turbulent production due to shear. The normalized profiles of energy dissipation showed a slight increase in the energy dissipation rate with instability for cases III and IV, whereas, the energy dissipation rate was increased with a decrease in instability for cases I and II.

5. Conclusions

An experimental study was conducted to investigate the impact of wall heating on the flow structure in the near-wall region inside a square channel. The results have shown that when a flow is unstably stratified via heating through a bottom wall, both the mean and turbulent characteristics are affected. The results have shown that the impact of wall heating on the flow behavior is significantly different for laminar and turbulent flow regimes. The instability due to buoyancy effects is quantified in terms of the gradient Richardson number. It was found that when a flow that is originally laminar is heated from below, the mean streamwise velocity in the near-wall region is significantly increased and turbulence is generated in the flow. The turbulence production due to the mean shear in this flow regime is negligible and the turbulence production is predominantly due to buoyancy. Thus, a flow that is originally laminar becomes turbulent with the heat addition. However, when the flow is in the turbulent regime, addition of heat from below reduces the magnitudes of mean streamwise velocity and turbulent properties. The reduction in the magnitudes of turbulent properties in this flow regime is due to the working of turbulence against the buoyancy forces. The impact of instability in stratification was also investigated. The results have shown that the instability in stratification has different impact on the turbulent characteristics for originally laminar and originally turbulent flows. For originally laminar flows, the turbulence is increased with an increase in instability, whereas, for originally turbulent flows, the turbulence is decreased with an increase in instability.

Acknowledgements

This research was funded by Grants from the Natural Sciences and Engineering Research Council of Canada (RGPIN 261422-03) and Concordia University to M.H. Kamran Siddiqui. The authors would like to thank Dr. Mark Loewen for providing the laser.

References

Ameel, T.A., 1997. Average effects of forced convection over a flat plate with an unheated starting length. International Communications in Heat and Mass Transfer 24, 1113–1120.

Arya, S.P.S., 1975. Buoyancy effects in a horizontal flat-plate boundary layer. Journal of Fluid Mechanics 68, 321–343.

Bakken, O.M., Krogstad, P.-A., Ashrafian, A., Andersson, H.I., 2005. Reynolds number effects in the outer layer of the turbulent flow in a channel with rough walls. Physics of Fluids 17, 065101.

Bergstrom, D.J., Kotey, N.A., Tachie, M.F., 2002. The effects of surface roughness on the mean velocity profile in a turbulent boundary layer. Journal of Fluids Engineering 124, 664–670.

Del Alamo, J.C., Jimenez, J., Zandonade, P., Moser, R.D., 2004. Scaling of the energy spectra of turbulent channels. Journal of Fluid Mechanics 500, 135–144.

Doron, P., Bertuccioli, L., Katz, J., Osborn, T.R., 2001. Turbulence characteristics and dissipation estimates in the coastal ocean bottom boundary layer from PIV data. Journal of Physical Oceanography 31, 2108–2134.

Fukui, K., Nakajima, M., 1985. Unstable stratification effects on turbulent shear flow in the wall region. International Journal of Heat and Mass Transfer 28, 2343–2352.

Gerard, R., 1974. Turbulent flow near smooth wall. ASCE Journal of Engineering Mechanical Division 100, 1129–1142.

Hirota, M., Fujita, H., Yokosawa, H., Nakai, H., Itoh, H., 1997. Turbulent heat transfer in a square duct. International Journal of Heat and Fluid Flow 18, 170–180.

Ichimiya, K., Yamada, Y., 2005. Mixed convection in a horizontal square duct with local inner heating. Heat Transfer – Asian Research 34, 160–170.

Krogstad, P.-A., Anotonia, R.A., Browne, L.W.B., 1992. Comparison between rough- and smooth-wall turbulent boundary layers. Journal of Fluid Mechanics 245, 599–617.

Na, Y., Hanratty, T.J., Liu, Z.-C., 2001. The use of DNS to define stress producing events for turbulent flow over a smooth wall. Flow, Turbulence and Combustion 66, 495–512.

Nicholl, C.I.H., 1970. Some dynamical effects of heat on a turbulent boundary layer. Journal of Fluid Mechanics 40, 361–384.

Perry, A.E., Hoffmann, P.H., 1976. An experimental study of turbulent convective heat transfer from a flat plate. Journal of Fluid Mechanics 77, 355–368.

Perry, A.E., Lim, K.L., Henbest, S.M., 1987. An experimental study of the turbulence structure in smooth- and rough-wall boundary layers. Journal of Fluid Mechanics 177, 437–466.

Rued, K., Murthy, J.Y., Metzger, D.E., 1987. Turbulent convection heat transfer at the corner intersection of heated and unheated walls in a square channel. ASME, HTD 87, 49–55.

Siddiqui, M.H.K., Loewen, M.R., Richardson, C., Asher, W.E., Jessup, A.T., 2001. Simultaneous particle image velocimetry and infrared imagery of microscale breaking waves. Physics of Fluids 13, 1891–1903.

Tennekes, H., Lumley, J.L., 1972. A First Course in Turbulence. MIT press.

Townsend, A.A., 1958. The effects of radioactive transfer on turbulent flow of a stratified fluid. Journal of Fluid Mechanics 4, 361–375.

Townsend, A.A., 1976. The Structure of Turbulent Shear Flow. Cambridge University Press, Cambridge.

Turner, J.S., 1973. Buoyancy Effects in Fluids. Cambridge University Press, New York, N.Y.